NeuroImage 230 (2021) 117810

Contents lists available at ScienceDirect

NeuroImage

journal homepage: www.elsevier.com/locate/neuroimage

Imaging iron and neuromelanin simultaneously using a single 3D gradient echo magnetization transfer sequence: Combining neuromelanin, iron and the nigrosome-1 sign as complementary imaging biomarkers in early stage Parkinson's disease

Naying He[a,+,*], Kiarash Ghassaban[b,c,+], Pei Huang[d,+], Mojtaba Jokar[e], Ying Wang[b,e], Zenghui Cheng[a], Zhijia Jin[a], Yan Li[a], Sean K. Sethi[b,e], Yixi He[d], Yongsheng Chen[f], Sara Gharabaghi[e], Shengdi Chen[d,*], Fuhua Yan[a,*], E. Mark Haacke[a,b,c,e,f]

[a] Department of Radiology, Ruijin Hospital, Shanghai Jiao Tong University School of Medicine, China
[b] Department of Radiology, Wayne State University, 3990 John R, Detroit, Michigan 48201, USA
[c] Department of Biomedical Engineering, Wayne State University, 3990 John R, Detroit, Michigan 48201, USA
[d] Department of Neurology, Ruijin Hospital, Shanghai Jiao Tong University School of Medicine, Shanghai, China
[e] SpinTech, Inc., Bingham Farms, Michigan 48025, USA
[f] Department of Neurology, Wayne State University, 4201 St. Antoine, Detroit, Michigan 48201, USA

ARTICLE INFO

Keywords:
Parkinson's disease
Substantia nigra
Neuromelanin
Nigrosome-1 sign
Magnetization transfer contrast
Quantitative susceptibility mapping

ABSTRACT

Diagnosing early stage Parkinson's disease (PD) is still a clinical challenge. Previous studies using iron, neuromelanin (NM) or the Nigrosome-1 (N1) sign in the substantia nigra (SN) by themselves have been unable to provide sufficiently high diagnostic performance for these methods to be adopted clinically. Our goal in this study was to extract the NM complex volume, iron content and volume representing the entire SN, and the N1 sign as potential complementary imaging biomarkers using a single 3D magnetization transfer contrast (MTC) gradient echo sequence and to evaluate their diagnostic performance and clinical correlations in early stage PD. A total of 40 early stage idiopathic PD subjects and 40 age- and sex-matched healthy controls (HCs) were imaged at 3T. NM boundaries (representing the SN pars compacta (SNpc) and parabrachial pigmented nucleus) and iron boundaries representing the total SN (SNpc and SN pars reticulata) were determined semi-automatically using a dynamic programming (DP) boundary detection algorithm. Receiver operating characteristic analyses were performed to evaluate the utility of these imaging biomarkers in diagnosing early stage PD. A correlation analysis was used to study the relationship between these imaging measures and the clinical scales. We also introduced the concept of NM and total iron overlap volumes to demonstrate the loss of NM relative to the iron containing SN. Furthermore, all 80 cases were evaluated for the N1 sign independently. The NM and SN volumes were lower while the iron content was higher in the SN for PD subjects compared to HCs. Interestingly, the PD subjects with bilateral loss of the N1 sign had the highest iron content. The area under the curve (AUC) values for the average of both hemispheres for single measures were: .960 for NM complex volume; .788 for total SN volume; .740 for SN iron content and .891 for the N1 sign. Combining NM complex volume with each of the following measures through binary logistic regression led to AUC values for the averaged right and left sides of: .976 for total iron content; .969 for total SN volume, .965 for overlap volume and .983 for the N1 sign. We found a negative correlation between SN volume and UPDRS-III (R^2 = .22, p = .002). While the N1 sign performed well, it does not contain any information about iron content or NM quantitatively, therefore, marrying this sign with the NM and

Abbreviation: PD, Parkinson's disease; HC, healthy control; MTC, magnetization transfer contrast; QSM, quantitative susceptibility mapping; NM, neuromelanin; UPDRS-III, unified Parkinson's disease rating scale part-III; AUC, area under the curve; H&Y, Hoehn and Yahr; SN, substantia nigra; SNpc, substantia nigra pars compacta; SNpr, substantia nigra pars reticulata; VTA, ventral tegmental area; PBP, parabrachial pigmented nucleus; SNpd, substantia nigra pars dorsalis; SN_{VOLMTC}, the SNpc and VTA volume measured from the MTC data in mm^3; SN_{VOLQSM}, the total SN volume (SNpc plus SNpr) measured on MTC-QSM in mm^3; $SN_{\Delta\chi}$, the volumetric mean susceptibility from MTC-QSM in ppb; $SN_{OVERLAP}$, the intersection of the $SN_{VOL,MTC}$ and $SN_{VOL,QSM}$ normalized to $SN_{VOL,QSM}$ in %.

* Corresponding authors.
+ These three authors made equal contributions.
E-mail addresses: i@nayinghe.com (N. He), ruijincsd@126.com (S. Chen), yfh11655@rjh.com.cn (F. Yan).

https://doi.org/10.1016/j.neuroimage.2021.117810
Received 31 October 2020; Received in revised form 15 January 2021; Accepted 23 January 2021
Available online 30 January 2021

iron measures provides a better physiological explanation of what is happening when the N1 sign disappears in PD subjects. In summary, the combination of NM complex volume, SN volume, iron content and the N1 sign as derived from a single MTC sequence provides complementary information for understanding and diagnosing early stage PD.

Introduction

Parkinson's disease (PD) is one of the fastest growing neurodegenerative disorders in the world and a leading cause of disability. Early PD diagnosis is still challenging and motivates an increasing need for non-invasive imaging biomarkers. Although Datscan can be used as an absolute exclusion criterion for diagnosing PD (Berg et al., 2018), it is not widely available, it is expensive, and it uses radioisotopes.

PD is characterized by the classical motor features of parkinsonism with early prominent death of dopaminergic neurons in the substantia nigra pars compacta (SNpc). The SNpc (referring to the dorsal part of the SN) and the SN pars reticulata (SNpr, referring to the ventral part of the SN) are anatomically and functionally distinct (see **Supplementary section S1** for further anatomical details). The SNpr contains higher levels of iron than the SNpc in normal subjects, while the SNpc is rich in dopaminergic neurons which are known to accumulate neuromelanin (NM). Consequently, in most previous neuroimaging studies (Lehericy et al., 2014), the SNpr is usually detected as a T_2^*W hypointense region due to high iron content while the SNpc has both hypointense regions with high iron and hyperintense regions such as the nigrosome-1 NM rich area (due to its high T_2^* values and lower iron content) as validated in NM-sensitive MRI (NM-MRI). (Langley et al., 2017) As a result, while the SNpc is characterized by NM content, the SNpr is usually responsible for regional high iron content in the SN. Practically, it is very difficult to differentiate SNpr and SNpc with MRI. However, similar to other major deep gray matter nuclei of the brain, and complicating the issue, is the fact that total iron content in the SN increases as a function of age with a relatively large spread in values. (Liu et al., 2016; Sethi et al., 2019)

Anatomically, the NM-containing dopaminergic neurons are not restricted to the SNpc region. According to histological studies (Yetnikoff et al., 2014), the dopaminergic neurons in the midbrain are located in three different groups referred to as A8, A9 and A10. Apart from the SNpc (group A9), the overall ventral tegmental area (VTA) region (located in A8 and A10) contains dopaminergic neurons. (Lehericy et al., 2014) The parabrachial pigmented nucleus (PBP) or SN pars dorsalis (SNpd) is located ventromedially to dorsolaterally between the red nucleus and the SNpc while the VTA nucleus lies ventral to the RN at the ventromedial limit of the PBP. The PBP together with the midline VTA nucleus constitute the dorsal tier of the dopaminergic neurons in the midbrain. Due to the variability of anatomical and neurochemical properties within the overall VTA region, it is difficult to separate the SNpc and the overall VTA region both histologically in humans and in-vivo on MR images. (Trutti et al., 2019) However, using multi-contrast MRI, particularly using QSM, it is possible to differentiate the SNpc from the overall VTA region as a whole. (Lee et al., 2018) A schematic of the midbrain summarizing these structures is shown in **Fig. 1**.

It is believed that dopaminergic neuronal death in the SNpc is followed by NM depigmentation leaving behind iron that is then phagocytized and becomes visible in MRI (Sulzer et al., 2018). Therefore, the most promising clinical MR biomarker candidates are iron content as seen with R_2^* or quantitative susceptibility mapping (QSM) (Ghassaban et al., 2019) and NM as measured with NM-MRI (Pavese and Tai, 2018). QSM provides a quantitative measure of the iron in the total SN, including the SNpc and SNpr, while the hyperintense signal seen in NM-MRI is spatially associated with the SNpc and the overall VTA region inclusive of the SNpd as well as with the NM seen in post-mortem histological studies (Keren et al., 2015). It has been shown that the MRI representation of NM matches the dopaminergic territory seen in PET and that the intensity of the NM signal in MRI correlates with the dopamine release capacity (Cassidy et al., 2019). The literature generally supports the concept that iron content is expected to increase in the SNpc in PD subjects while NM is expected to decrease in PD subjects (Peran et al., 2010; Takahashi et al., 2018a; Takahashi et al., 2018b). An alternate approach that does not measure NM throughout the SN but rather is sensitive to just the NM in the nigrosome-1 (N1) territory has also been promoted as a possible means to discriminate between PD subjects and healthy controls (HC) (Cheng et al., 2020; Mahlknecht et al., 2017; Pavese and Tai, 2018). The disappearance of the N1 sign is a surrogate marker to the loss of NM overall as well as an increase in local iron content (Blazejewska et al., 2013), but this approach does not actually measure NM or iron content quantitatively. However, the sensitivity and specificity of either NM, iron or the N1 sign in the SN may not be good enough for them to qualify as diagnostic biomarkers by themselves (Takahashi et al., 2018a; Takahashi et al., 2018b; Wang et al., 2019).

Some studies have combined NM and iron measures, but they used two different sequences which required co-registration and data interpolation (Isaias et al., 2016; Lee et al., 2018; Reimao et al., 2016; Takahashi et al., 2018a; Takahashi et al., 2018b) and, sometimes, the use of a NM template mask (Langley et al., 2017). Only one group used a single two-echo 2D gradient echo (GRE) sequence to study NM and susceptibility weighted imaging (SWI) (Langley et al., 2015). Apart from the volume and intensity measures of SN or NM usually used in PD neuroimaging studies, a prior study (He et al., 2020) showed that the overlap between the iron content as determined by R_2^* mapping and the neuromelanin mask of the SNpc provided good diagnostic performance to differentiate PD from HC. Also, during the past few years, the N1 sign which is usually imaged with a 3D SWI scan (Cheng et al., 2020) is gaining attention as a potential imaging biomarker of pathophysiologic changes in PD subjects. Our hypothesis is that the combination of these imaging measures will provide a comprehensive understanding of the pathophysiological changes in the SN underlying PD and outperform each single measure by themselves.

Therefore, our goal was to use a single sequence to evaluate four metrics as imaging biomarkers to differentiate early stage PD subjects from HCs: the NM complex volume (SNpc plus PBP), SN volume (SNpc plus SNpr), SN iron content (as measured using susceptibility in QSM) and the N1 sign. This innovative approach uses a 3D multi-echo, magnetization transfer contrast (MTC) GRE sequence that can be run in a clinical setting in less than 5 min.

Materials and methods

Subjects

This study was approved by the local ethics committee at Ruijin Hospital and consent forms were signed by all subjects. Forty subjects with early stage idiopathic PD and 40 sex- and age-matched HCs were recruited from the Ruijin movement disorder clinic and local advertisements from May 2018 to January 2019. All subjects were on medication. The diagnosis and severity of motor symptoms were assessed by two neurologists based on the Movement Disorders Society (MDS) PD criteria (Berg et al., 2018), the Hoehn & Yahr (H&Y) stage and the MDS Unified Parkinson's Disease Rating Scale Part-III (UPDRS-III) (Goetz et al., 2008). Symptom laterality was determined by measuring the difference between the right and left UPDRS-III sub scores (Barrett et al., 2011) The exclusion criteria of PD were as follows: (1) H&Y scale more than

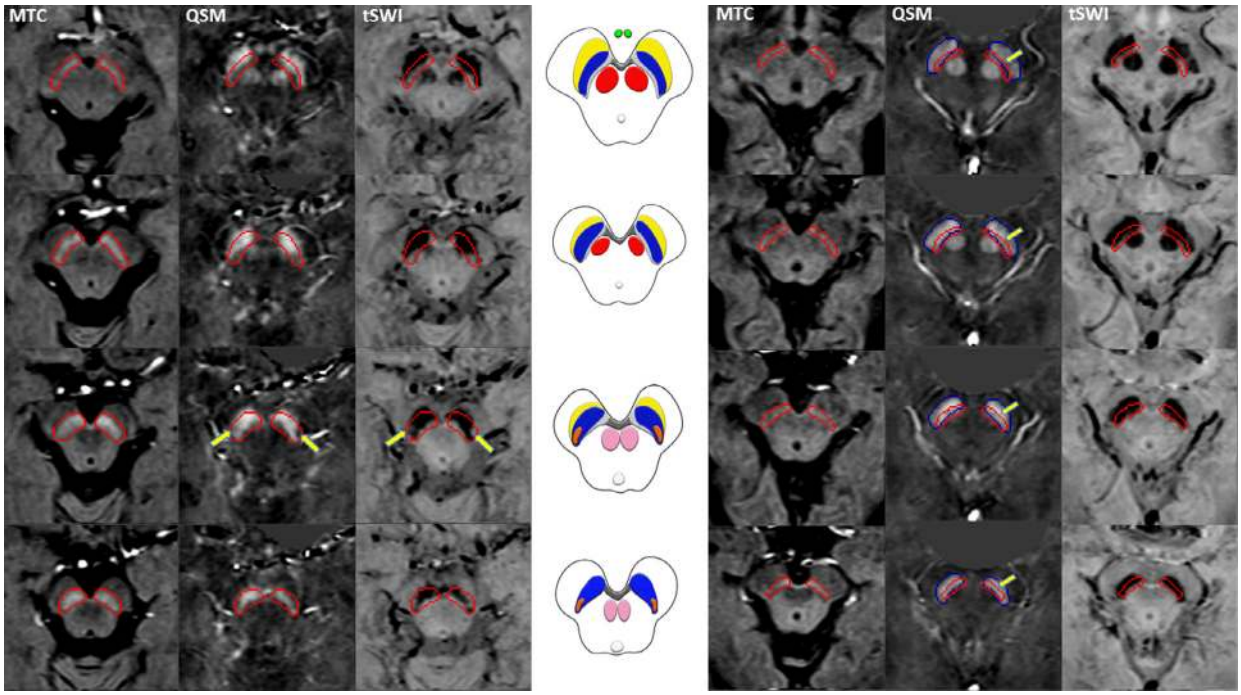

Fig. 1. Neuromelanin, iron and N1 in the SN as represented by MTC magnitude, MTC-QSM and MTC-tSWI data. From left to right, the first three columns show four consecutive slices from a 63-year-old healthy control followed by the schematic of different midbrain structures and the same contrasts from a 62-year-old PD subject shown in the last three columns. The top and bottom rows show the most rostral and most caudal slices, respectively. The red ROIs representing the NM complex were drawn on the MTC magnitude data and then overlaid on the corresponding MTC-QSM and MTC-tSWI datasets. It should be noted that the overlap between the NM complex and the iron containing SN (i.e., the SNpc in controls) increases towards the caudal slices in the HC subject while this area is substantially smaller in the PD subject on a slice-by-slice basis. The yellow arrows in the second and third columns show the N1 territory located in the ventral-lateral aspect of the NM complex while the yellow arrows in the right column represent the directionality of the NM loss (and overlap) starting from the ventral tier and continuing towards the dorsal tier of the SNpc. The regions shown by the NM boundaries but that lie outside the SN as highlighted in the QSM data represent the PBP (also known as the SNpd). The highlighted regions in the schematic represent: green: mammillary bodies; pink: superior cerebellar peduncles; red: red nucleus, orange: Nigrosome-1 territory; yellow: SN pars reticulata (SNpr); blue: SN pars compacta (SNpc); light gray: SN pars dorsalis (SNpd)/parabrachial pigmented nucleus (PBP); and dark gray: ventral tegmental area (VTA) nucleus.

2.5; (2) Mini-Mental State Examination (MMSE) score less than 24; (3) a history of cerebrovascular disease, brain tumor, head trauma or any other type of psychiatric disorders; (4) a history of medication known to cause parkinsonism or affect clinical assessment; (5) contraindications to an MRI examination, and (6) younger than 40 years of age. The inclusion criteria for the HCs were as follows: (1) no family history of movement disorders; (2) no neurological or psychiatric disorders; (3) an MMSE score of at least 24 and (4) older than 40 years of age. PD subjects were evaluated one year later to confirm the diagnosis using the same MDS-PD diagnostic criteria as used at the baseline for PD diagnosis.

MRI data collection

All data were collected on a 3T Ingenia scanner (Philips Healthcare, Netherlands) using a 15-channel head coil. A seven-echo 3D SWI sequence with an MTC pulse was collected using: TE = 7.5 ms and ΔTE = 7.5 ms, TR = 62 ms, flip angle = 30°, pixel bandwidth = 174 Hz/pixel, matrix size = 384 × 144, slice thickness = 2 mm, in-plane resolution = 0.67 mm × 1.34 mm and total scanning time = 4 min 47 s for 64 slices. The MTC pulse was an on-resonance (Stoeck et al., 2010) 90° flip angle with 3 block pulses of 1.91 ms which is part of the Philips product sequence (Liu et al., 2020). To validate that the phase images from the MTC scan can also provide normative QSM data, a separate multi-echo SWI sequence was acquired as part of the strategically acquired gradient echo (STAGE) protocol (Chen et al., 2018; Haacke et al., 2020; Wang et al., 2018b) using: TEs = 7.5 and 17.5 ms, TR = 25 ms, flip angles = 6° and 24°, pixel bandwidth = 220 Hz/pixel, imaging matrix size = 384 × 144, slice thickness = 2 mm, an in-plane resolution = 0.67 mm × 1.34 mm and a scanning time of 1 min 53 s for 64 slices per scan. In both cases, the images were interpolated to an in-plane resolution of 0.67 mm × 0.67 mm. The axial slice orientation was the anterior commissure to posterior commissure (ACPC) line for all scans.

Data processing and analysis

MTC and QSM data

The NM signal was evaluated from the first echo (TE = 7.5 ms) of the MTC data while the susceptibility maps (denoted as MTC-QSM) were calculated using the second echo (TE = 15 ms) data to avoid more severe aliasing at the longer echo times. The MTC-QSM process included the following steps: a brain extraction tool was applied (threshold = 0.2, erode = 4 and island = 2000) Smith (2002) using the first echo magnitude data; a 3D phase unwrapping algorithm (3D sorting by reliability following a non-continuous path or 3DSRNCP) was used to unwrap the original phase data (Abdul-Rahman et al., 2007); sophisticated harmonic artifact reduction (SHARP) was used to remove unwanted background fields (threshold = 0.05 and deconvolution kernel size = 6) (Schweser et al., 2011); and a truncated k-space division based inverse filtering technique (threshold = 0.1) (Haacke et al., 2010) was used with an iterative approach (iteration threshold = 0.1 and number of iterations = 4) to reconstruct the susceptibility maps (Tang et al., 2013). The same QSM processing pipeline was used to reconstruct the second echo (TE = 17.5 ms) data from the STAGE sequences, denoted as STAGE-QSM. Finally, the MTC-QSM and the magnitude image of the second

echo were used to create true SWI (tSWI) data for the detection of the N1 sign. (Liu et al., 2014)

Defining the NM and iron boundaries and quantification of volumes and susceptibility

Two sets of regions of interest (ROIs) were outlined separately one for NM on the MTC images and one for iron on the MTC-QSM images. The images were zoomed by a factor of four to more easily and accurately draw the boundaries for NM and iron. The iron-based SN ROIs were traced starting from one slice below the most cranial slice where the subthalamic nucleus was visible and continued for four to five consecutive slices to the most caudal slice. The NM boundaries, however, were traced from the last caudal slice (which corresponds to the most caudal slice showing iron content in the SN) for four to five slices cranially until the NM was no longer visible as shown in **Fig. 1**. The NM complex used in this study was defined as the region showing NM contrast in the midbrain but excluding the midline VTA nucleus (as shown in the central dark gray area in **Fig. 1** fourth column). Finding the final boundaries was done with a two-step process. First, all initial input boundaries were reviewed by three raters and then an intermediate set of boundaries was chosen by consensus. These boundaries were initially traced a few pixels outside what would have otherwise been drawn manually by any of the raters while avoiding the hyperintense structures such as veins outside the desired final ROI. Second, to remove the human element completely, a dynamic programming algorithm was used to determine the final boundaries (Jiang et al., 2007) (see **Supplementary section S2** and **Supplementary Fig. 3** for more details). This semi-automated approach provides a means to generate a mathematically determined user independent boundary. DICE similarity coefficients associated with different sets of results from the raters before reaching consensus were calculated as .89 and .84 for the $SN_{VOL,MTC}$ and .91 and .88 for the $SN_{VOL,QSM}$ in the HC and PD subjects, respectively. A partial volume correction of the most caudal slice was performed on the NM, QSM and overlap fraction data. The partial volume effect was calculated based on the contrast of the most caudal slice and of the second and third most caudal slices via:

$$\begin{aligned} &Volume\ of\ the\ slice\ with\ partial\ volume\ effect \\ &= measured\ volume\ of\ the\ slice \\ &\times \frac{contrast\ of\ the\ slice}{average\ contrast\ of\ the\ two\ middle\ slices} \end{aligned}$$

A volumetric analysis was performed using the boundaries from all slices covering both the NM and iron containing SN. The results were then compared between the PD and HC groups as well as between the two hemispheres for each group for the NM complex and iron containing SN total volumes. The overlap between the NM complex volume (SNpc plus PBP) and iron containing SN volume (SNpc plus SNpr) was evaluated by superimposing the two ROIs from the MTC and MTC-QSM data, respectively. This overlap was normalized by the iron containing SN volume creating an overlap fraction measure which basically represents the SNpc fraction with respect to the entire SN volume (**Fig. 1**), as given below:

$$\begin{aligned} &Overall\ Overlap\ Fraction \\ &= \frac{\sum_{slices\ where\ SN_{pc}\ is\ present} volume\ of\ the\ intersection\ between\ NM\ and\ SN}{\sum_{slices\ where\ SN_{pc}\ is\ present} volume\ of\ the\ iron\ containing\ SN} \end{aligned}$$

For ease of reference, hereafter we define $SN_{VOL,MTC}$ as the SNpc plus PBP volume measured from the MTC data in mm^3; $SN_{VOL,QSM}$ as the total SN volume (SNpc plus SNpr) measured on MTC-QSM in mm^3; $SN_{\Delta\chi}$ as volumetric mean susceptibility from MTC-QSM in ppb; and $SN_{OVERLAP}$ as the intersection of the $SN_{VOL,MTC}$ and $SN_{VOL,QSM}$ normalized to $SN_{VOL,QSM}$ in percent.

The mean susceptibility of the SN was measured and compared between the two groups in both hemispheres. These global values were plotted as a function of age against the corresponding baselines from a normal population established by Liu et al. (Liu *et al.*, 2016). To demonstrate that MTC-QSM and the normative STAGE-QSM (without the MT pulse) are equivalent to each other, the same SN boundaries traced on MTC-QSM were superimposed on the STAGE-QSM data for the HCs. The two datasets were acquired with the same resolution and brain coverage and the magnitude images were aligned to each other using SPM software (V12, Functional Imaging Laboratory, UCL, London, UK), and the QSM data were then transformed according to the geometric displacement matrix. For each case, the mean susceptibility was extracted from the whole 3D ROI and averaged over the two hemispheres. A linear regression model was applied to evaluate the correlation between the averaged mean susceptibility between these two sequences for all the HCs and PD subjects. (see **Supplementary section S3**)

In order to assess the potential dependence of volumetric analyses to brain tissue atrophy and spread of the data in both cohorts, a normalization of $SN_{VOL,MTC}$ and $SN_{VOL,QSM}$ to the whole midbrain volume was done by manually tracing 3D boundaries on the first echo magnitude data. (see **Supplementary section S6**)

N1 sign evaluation

The N1 sign evaluation (no loss, unilateral loss or bilateral loss) was performed in a blinded manner using the MTC-tSWI data (which has been found to be the best modality to show the N1 sign in previous works) (Cheng et al., 2020; Nam et al., 2017) and the MTC-QSM data by two reviewers separately. The consensus results between the two reviewers were then used for the final analyses. To validate the interpretation of the data, each slice where the N1 sign was found was compared with the boundaries from the MTC data to ensure that the interpretation of the N1 sign was correct in that it was situated in the ventral-lateral side of the NM complex. This has not been possible previously when just using QSM by itself as the N1 sign is usually recognized either by the swallowtail or ovoid sign and a hyperintense area remaining inside. Using the MTC boundaries assures a correct interpretation of the data.

Statistical analysis

Subject characteristics are presented as mean ± standard error of the mean (SEM). Two-sample and paired t-tests were used for inter-group comparisons between the two groups and intra-group comparisons between the two hemispheres as well as the comparison between the ipsilateral and contralateral sides in the PD group, respectively. The area under the curve (AUC) for receiver operating characteristic (ROC) analysis was calculated to evaluate the overall diagnostic performance of the $SN_{\Delta\chi}$, $SN_{VOL,QSM}$, $SN_{VOL,MTC}$ and $SN_{OVERLAP}$, as independent predictors. Then, the diagnostic performances for PD were compared using the DeLong test. Binary logistic regression was used to integrate information from different combinations of these measures to produce associated ROC curves. We performed partial correlation analysis to explore relationships between each image feature and the clinical variables (disease duration and UPDRS-III) using age and sex as covariates. All statistical analyses were performed using IBM SPSS Statistics Version 25 (International Business Machines Corporation, Armonk, NY, USA). A p-value < .05 for two-sided tests was considered significant. The Bonferroni correction was used to correct the partial correlations when multiple comparisons were used in the correlation analyses (p-value threshold for significance: .006) and ROC comparisons (p-value threshold for significance: .003).

Results

Demographic and clinical characteristics are shown in **Table 1**. There was no significant difference in sex or age between the two groups. For any of the imaging measures discussed herein, there were no significant differences between the ipsilateral and contralateral side for the PD group, or between the left side and right side for the HC group.

Table 1
Demographic and clinical characteristics of Parkinson's disease and healthy control groups.

	Parkinson's disease	Healthy controls	*p*-value
Sex, man:woman	20:20	20:20	-
Age, years[a]	63.10 ± 8.05 [43–76]	65.50 ± 8.19 [44–81]	.19
Disease duration, years	2.55 ± 2.92 [0.08–15]		
UPDRS-III	22.73 ± 14.26 [6–64]		
Hoehn and Yahr scale	1.78 ± 0.52 [1–2.5]		
Symptom laterality, left:right	14:26		

Values represent mean ± standard deviation [range]. The UPDRS-III was administered while subjects were in the ON medicated state. [a]Significant differences were tested using independent t-test.

NM complex and iron containing SN volume comparison between early stage PD subjects and healthy controls

An example set of the slices evaluated is shown pictorially in **Fig. 1**. These boundaries were used to calculate $SN_{VOL,MTC}$ and $SN_{VOL,QSM}$. The $SN_{VOL,MTC}$ were (322.85 ± 4.72) mm^3 and (234.58 ± 6.22) mm^3 averaged between the right and left hemispheres of the HC and PD groups, respectively. This example also highlights the fact that the N1 sign shown in the caudal slices lies within the ventral-lateral tier of the NM boundary. The PD group had significantly lower NM complex volumes than those of the HC group ($p < .001$). There was no significant correlation of $SN_{VOL,MTC}$ with age for either group. (see **Supplementary section S4** and **Supplementary Fig. 6**) The $SN_{VOL,QSM}$ were (477.53 ± 12.63) mm^3 and (395.38 ± 9.61) mm^3 averaged over the right and left hemispheres of the HC and PD groups, respectively, with the PD group showing lower volumes ($p < .001$). There was a decreasing trend in $SN_{VOL,QSM}$ as a function of age (**Supplementary Fig. 6**) which reached significance for PD ($p = .001$) but not for HCs ($p = .070$). The mean $SN_{OVERLAP}$ values were (39.96 ± 1.05)% and (36.49 ± 1.29)% averaged over the right and left hemispheres of the HC and PD groups, respectively, with the PD group showing lower overlap percentages ($p = .040$) (**Supplementary Table 1**). There were no significant differences between male and female results in any of the measures ($p > .050$ in all cases).

The scatter plots for $SN_{VOL,MTC}$ versus $SN_{OVERLAP}$, $SN_{VOL,QSM}$ and $SN_{\Delta\chi}$ are presented in **Fig. 2A-C**, respectively. **Fig. 2A** shows the $SN_{VOL,MTC}$ as a function of $SN_{OVERLAP}$ in all 4 to 5 slices where both NM and SN are present. However, there is a larger overlap of PD and HC cases between $SN_{VOL,MTC}$ and either $SN_{OVERLAP}$ or $SN_{VOL,QSM}$ (**Figs. 2A and 2B**) compared to that of $SN_{VOL,MTC}$ and $SN_{\Delta\chi}$ (**Fig. 2C**). The sensitivity, specificity and accuracy associated with the relationship between $SN_{VOL,MTC}$ and $SN_{\Delta\chi}$ (**Fig. 2C**) provided slightly better, although statistically insignificant, performance in separating the two cohorts compared to the other two metrics. ($p = .292$ comparing $SN_{VOL,MTC}/SN_{\Delta\chi}$ to $SN_{VOL,MTC}/SN_{OVERLAP}$ and $p = .470$ comparing $SN_{VOL,MTC}/SN_{\Delta\chi}$ to $SN_{VOL,MTC}/SN_{VOL,QSM}$).

Using MTC-QSM to quantify iron in PD

The relationship for the HCs between the two QSM approaches is shown in **Supplementary Fig.s 4** and **5 in Supplementary section S3**. The results confirm a strong positive relationship ($R^2 = .751$, $p < .001$, slope = 1.11, $p < .001$) between them indicating that MTC-QSM provides similar susceptibility values compared to the normative STAGE-QSM and, therefore, MTC-QSM is suitable to estimate regional brain iron levels.

SN iron deposition in PD

Using MTC-QSM, there was a higher iron content for early stage PD subjects compared to HCs in both hemispheres ($p < .001$). The data for the SN susceptibility analyses superimposed on the corresponding susceptibility-age baselines (Liu et al., 2016) are shown in **Fig. 3**. The $SN_{\Delta\chi}$ values were (132.12 ± 4.01) ppb and (155.30 ± 4.09) ppb averaged over the right and left hemispheres of the HC and PD groups, respectively, with the PD group showing higher $SN_{\Delta\chi}$ ($p < .001$). Not only did the PD group show higher iron content, within the PD group, the presence of bilateral loss of N1 sign was most evident in those cases with the highest iron content. Specifically, a total of 21 out of 25 PD cases on the right and 14 out of 15 cases on the left that lay above the 95% confidence interval for the iron distribution had bilateral loss of the N1 sign (**Fig. 3**). We also note that the more caudal the slice the more the NM overlaps with the iron (representing the SNpc) until at the last slice where it is almost a complete overlap showing that caudally the SN is predominantly the SNpc (see **Fig. 1**).

The added information from the N1 sign

The results from the N1 analysis reveal that 36 out of 40 HC cases showed bilateral presence of N1 while N1 loss, either unilaterally or bilaterally, was detected in 34 out of 40 PD cases. The N1 sign information included in **Fig. 2** shows that some PD cases that appear in the HC region are in fact bilateral loss of the N1 sign, making it possible to remove them from the HC region and further improve the sensitivity of the NM and SN volume. The N1 sign performed reasonably well by itself (AUC = .891) but was significantly improved when merged with $SN_{VOL,MTC}$ (AUC = .979; $p < .001$) and somewhat improved when merged with $SN_{\Delta\chi}$ (AUC = .953; $p = .056$). However when the N1 sign was merged with $SN_{VOL,MTC}$ and $SN_{VOL,QSM}$, the highest AUC of .983 ($p = .003$) was obtained.

Diagnostic performance for early stage PD

The AUC values associated with the average of the right and left hemispheres were .960 for the $SN_{VOL,MTC}$; .788 for the $SN_{VOL,QSM}$; .740 for the $SN_{\Delta\chi}$ and .629 for the $SN_{OVERLAP}$. However, combining the two QSM related measures, $SN_{VOL,QSM}$ and $SN_{\Delta\chi}$, yielded AUC values of .859 and adding $SN_{OVERLAP}$ brought these values to .911. Normalizing the $SN_{VOL,MTC}$ and $SN_{VOL,QSM}$ volumes to the whole midbrain volume did not improve the classification performance associated with any of the measured values. To support this claim, the *p*-values associated with the un-normalized versus normalized ROC curves corresponding to the combination of $SN_{VOL,MTC}$ with each of $SN_{VOL,QSM}$, $SN_{\Delta\chi}$ and $SN_{OVERLAP}$ were found to be .38, .36 and .49, respectively, indicating that the normalized data showed no significant improvement over the un-normalized data (see **Supplementary section S6 and Supplementary Fig. 9**).

The ROC curves associated with the $SN_{VOL,MTC}$, $SN_{VOL,QSM}$, $SN_{\Delta\chi}$ and $SN_{OVERLAP}$ are illustrated in **Fig. 4A**. As suggested in these plots and with respect to the above-mentioned AUC values, the $SN_{VOL,MTC}$ had a significantly higher AUC compared to those of the $SN_{VOL,QSM}$, $SN_{\Delta\chi}$ or $SN_{OVERLAP}$ for the average of the right and left hemispheres in differentiating early stage PD subjects from HCs ($p < .001$ for all), respectively (**Fig. 4A**). The ROC curves associated with the combination of $SN_{VOL,MTC}$

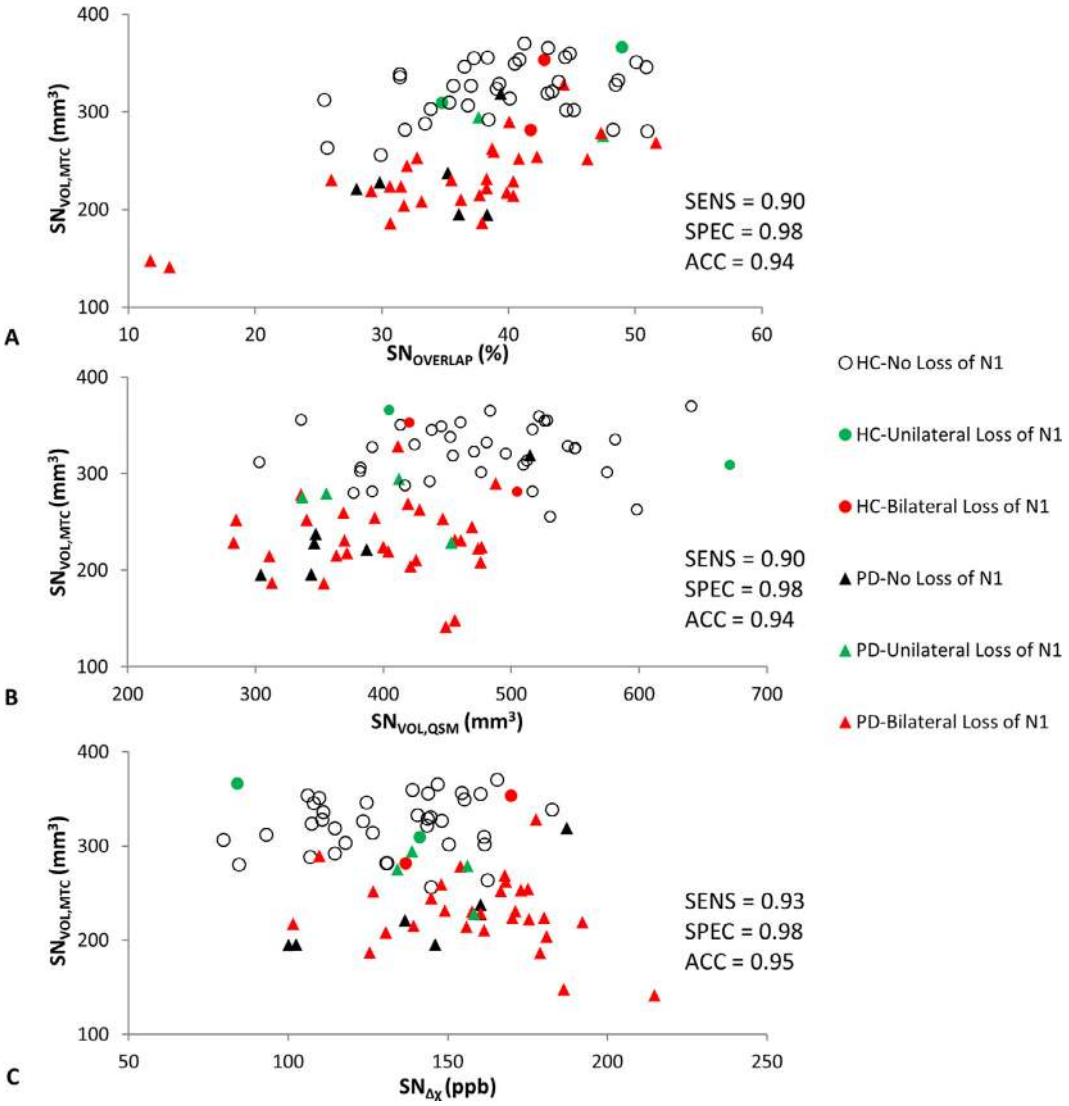

Fig. 2. Distinguishing between the two groups using NM complex volume and three other measures. $SN_{VOL,MTC}$ volume as a function of (A) $SN_{OVERLAP}$, (B) $SN_{VOL,QSM}$, and (C) $SN_{\Delta\chi}$. The data indicate the loss of N1 for both groups. Sensitivity (SENS), specificity (SPEC) and accuracy (ACC) values are also shown for each plot.

and the three other measures are shown in Fig. 4**B**. The corresponding AUC values were .969 for the combination of $SN_{VOL,MTC}$ and $SN_{VOL,QSM}$, .965 for $SN_{VOL,MTC}$ and $SN_{OVERLAP}$, and .976 for $SN_{VOL,MTC}$ and $SN_{\Delta\chi}$ for the average of the right and left hemispheres, respectively. The AUCs associated with all of the measure combinations are shown in **Supplementary Table 2**. Although we obtained a higher AUC value for the combination of all four measures than any individual measure, the difference was not significant ($p = .222$) compared to $SN_{VOL,MTC}$ alone, but was significant when compared to the rest of the individual measures ($p < .001$). Also, the AUC from the combination of $SN_{\Delta\chi}$ and $SN_{VOL,QSM}$ measures showed a low p value of .020 compared to $SN_{VOL,MTC}$ alone but not low enough to be significant at the .003 level **(see Supplementary Table 3)**.

Correlation analysis between imaging features and clinical scales

There was a significant loss of $SN_{VOL,QSM}$ with increasing UPDRS-III score ($R^2 = .22$, $p = .002$) (Fig. 5**A**). The correlation was not significant between the $SN_{\Delta\chi}$ and disease duration for the whole group ($R^2 = .12$, $p = .027$) (Fig. 5**B**), but there was a positive correlation between $SN_{\Delta\chi}$ and disease duration ($R^2 = .32$, $p < .001$) in the subgroup of PD patients with disease duration less than or equal to 5 years which is considered as early PD. (Berg et al., 2018) There were no other significant correlations with any of the other quantitative MRI measures with respect to clinical scales.

Discussion and Conclusion

To our knowledge, the integration of NM, iron, iron-NM overlap and the N1 sign derived from a single sequence to differentiate early stage PD from healthy controls has not been presented in the literature. In this study, the $SN_{VOL,MTC}$ provided the highest single measure diagnostic accuracy while the N1 sign provided the second highest diagnostic performance. Merging the $SN_{VOL,MTC}$ and $SN_{VOL,QSM}$ with the N1 sign yielded the highest AUC among all singular predictors and all combinations of predictors. We also found $SN_{VOL,QSM}$ negatively correlated with UPDRS-III and the $SN_{\Delta\chi}$ increased with disease duration in PD subjects during the first 5 years after showing clinical symptoms.

Previous studies have shown that diagnostic AUC for individual measures (NM contrast, $SN_{VOL,MTC}$, $SN_{\Delta\chi}$ and the width of SNpc) can vary from .65 to .92 (Castellanos et al., 2015; Huddleston et al., 2017; Isaias et al., 2016; Ogisu et al., 2013; Prasad et al., 2018; Reimao et al.,

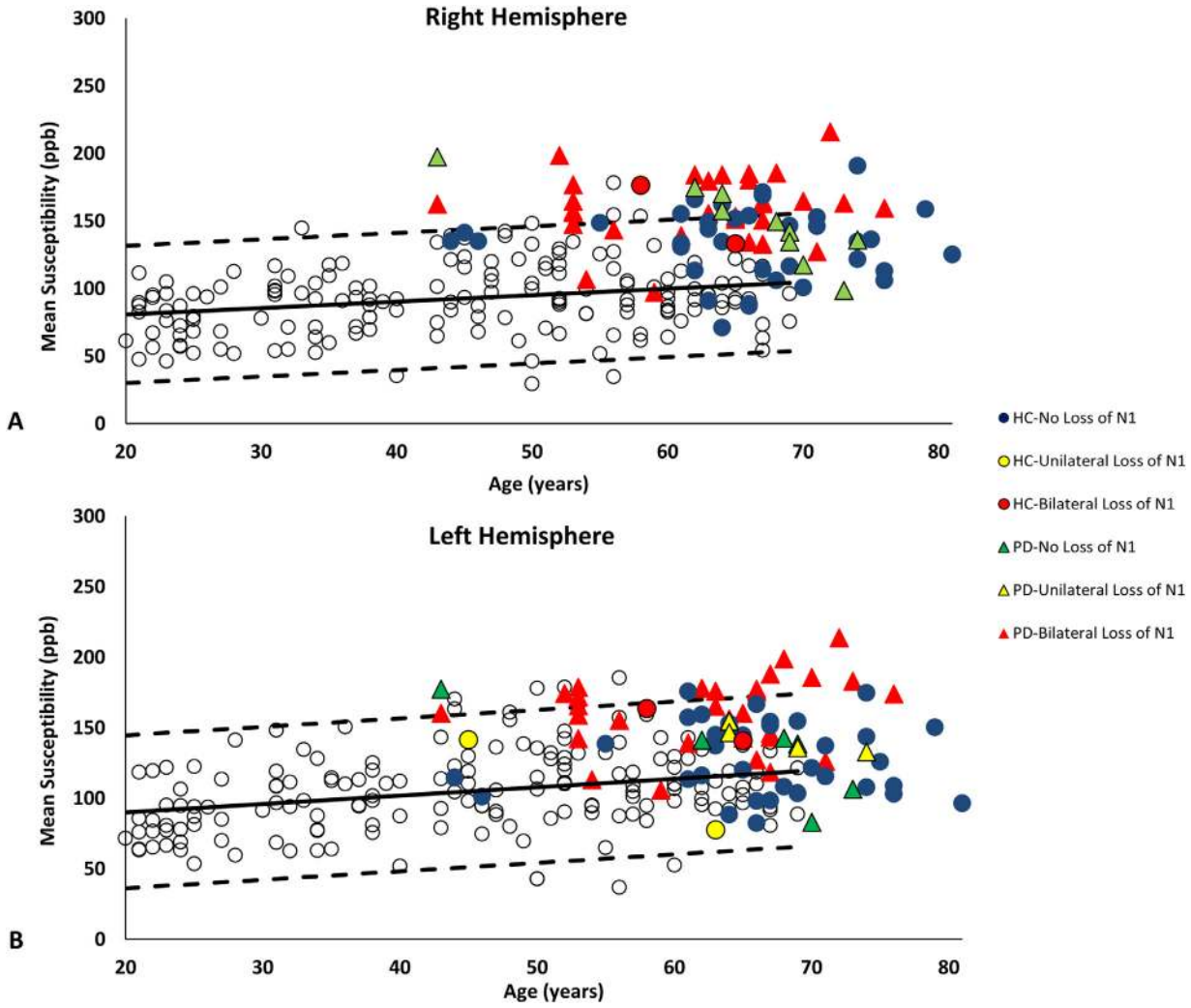

Fig. 3. Mean susceptibility as a function of age for a large normal population as well as HC and Parkinson's cases in this study. SN global iron content of the HC and Parkinson's disease groups associated with the (A) right and (B) left hemisphere. The bilateral, unilateral, and no loss of Nigrosome-1 for each group are also shown. The data are superimposed on the corresponding normal baselines established by Liu et al. illustrated by open circles. (Liu et al., 2016) The solid line and dashed lines show the linear regression model associated with the normal baseline and its corresponding 95% prediction intervals, respectively.

2015a; Reimao et al., 2015b; Shinde et al., 2019; Takahashi et al., 2018a; Takahashi et al., 2018b; Taniguchi et al., 2018) whereas our results for the combination of $SN_{VOL,MTC}$, $SN_{VOL,QSM}$, $SN_{\Delta\chi}$ and the N1 sign generated an AUC of up to .98. The main advantages of this single MTC sequence approach include: simultaneous NM and iron content information; rapid acquisition time (less than 5 min); no need for co-registration or the creation of templates; and high contrast data which is critical for boundary detection (Liu et al., 2020). Further, the semi-automated DP boundary detection approach we used in this study brought the boundaries traced by the raters in line with each other. This rapid approach to obtain both the iron and NM information simultaneously opens the door to its potential practical use in a clinical setting.

The results of this study showed an AUC for $SN_{\Delta\chi}$ and $SN_{VOL,QSM}$ measures together (which are both derived from QSM data) of .859 in differentiating early stage PD subjects from HCs. A similar approach comparing the NM and QSM data (but derived from two sequences) was used by Takahashi et al. using QSM and $SN_{VOL,MTC}$ derived from the SNpc component (VTA volumes removed); they found an AUC of .86 in both studies (Takahashi et al., 2018a; Takahashi et al., 2018b). The $SN_{OVERLAP}$ by itself performed poorly, likely due to the fact that the $SN_{VOL,MTC}$ and $SN_{VOL,QSM}$ can both be reduced leaving the overlap fraction invariant. On the other hand, it should be noted that even though under normal circumstances there is an almost complete overlap between $SN_{VOL,MTC}$ and $SN_{VOL,QSM}$ in the most caudal slice delineating the SNpc, the NM loss in PD patients appears to be happening mostly in the posterolateral aspect of the SNpc where the N1 territory is anatomically located.

Prior studies have shown that the N1 sign could be used to differentiate PD from HCs with reasonably good accuracy (Mahlknecht et al., 2017; Pavese and Tai, 2018). Although this method is attractive because of its visual nature in the images, it is not trivial as there is still overlap of the N1 appearance between PD subjects and HCs and none of the approaches introduced to date take the volume of the N1 sign into account (Cheng et al., 2020). Our study for the first time incorporated the N1 sign along with other quantitative measures such as the $SN_{VOL,MTC}$, $SN_{VOL,QSM}$, $SN_{OVERLAP}$ and $SN_{\Delta\chi}$ resulting in a comprehensive analysis of the pathological changes in PD. Although the N1 sign performs well by itself (AUC = .891), similar to the findings in Cheng et al (Cheng et al., 2020), it can be improved by combining this data with either $SN_{VOL,MTC}$, $SN_{VOL,QSM}$, or $SN_{\Delta\chi}$. This is not surprising since the N1 sign detection is not infallible. Further, the N1 sign does not quantitatively represent either iron or NM despite the fact that the absence of iron helps define the N1 sign appearance. We note that those PD cases with very high iron content turned out to show bilateral loss of the N1 sign. This is

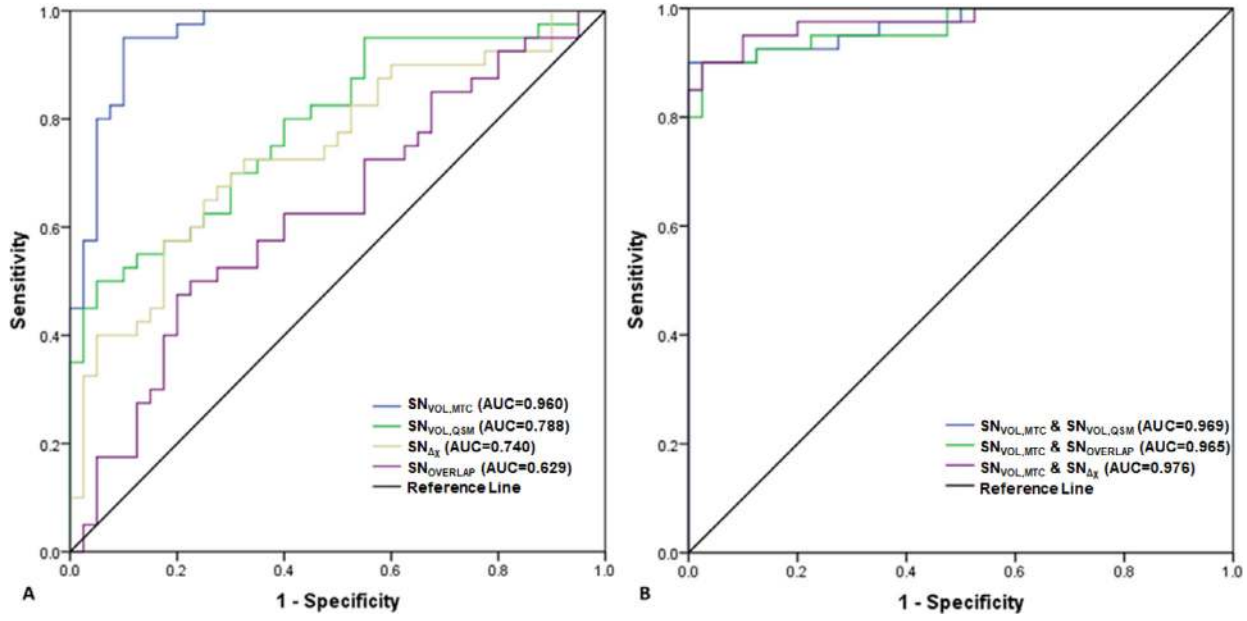

Fig. 4. ROC analyses of diagnostic performance using different neuroimaging measurements. (A) ROC analyses of the different combinations of NM complex volume ($SN_{VOL,MTC}$), SN volume ($SN_{VOL,QSM}$), global mean iron content ($SN_{\Delta\chi}$,) and overlap fraction ($SN_{OVERLAP}$) for the individual measures. (B) The combination of NM complex volume with the three other measures was calculated via a binary logistic regression analysis. The data are averaged over both hemispheres.

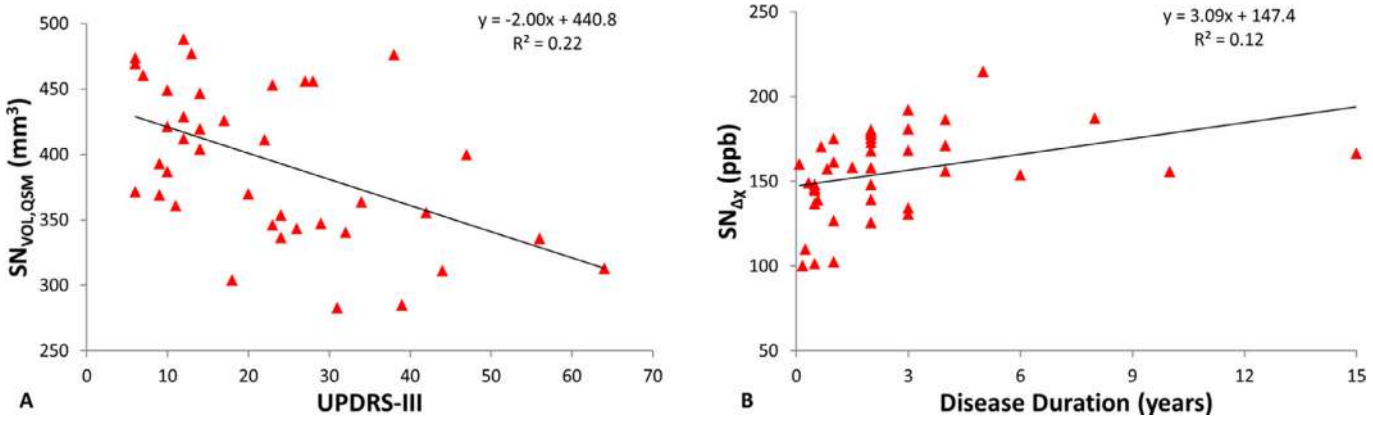

Fig. 5. The correlations of SN volume and iron content with clinical characteristics of Parkinson's disease. (A) $SN_{VOL,QSM}$ (averaged over both hemispheres) versus UPDRS-III. There is a significant reduction in the $SN_{VOL,QSM}$ as UPDRS-III increases (p = .002). (B) The correlation between $SN_{\Delta\chi}$ (averaged over both hemispheres) and disease duration in PD subjects (p = .027) is not significant after Bonferroni correction (p-value threshold for significance: .0125). There appears to be a rapid rise in the iron content in the first 5 years (with y = 11.8x + 133.4, R^2 = .32, and p < .001) and then it levels off for the early stage PD group.

not surprising either as the loss of the N1 sign is generally assumed to mean that there is higher iron content in that area (Cheng et al., 2020). Based on the aforementioned discussion, it is imperative to understand the role of each of these potential biomarkers by themselves. Ideally, in future studies, one may use all of this complementary information to have a more comprehensive picture of the pathology behind what is actually happening in the midbrain of PD patients in terms of volumetric changes, N1 loss and iron deposition.

We found a significant correlation between the $SN_{VOL,QSM}$ and UPDRS-III total score. A number of studies have also shown a negative association between clinical measures such as UPDRS-III and $SN_{VOL,MTC}$ (Isaias et al., 2016), area (Taniguchi et al., 2018) and width (Wang et al., 2018a). It should be noted that, from a pathological perspective, the loss of pigmented neurons in the SNpc is associated with disease duration and severity in PD (Fearnley and Lees, 1991) and that detecting atrophy of the contralateral SNpc side may allow earlier diagnosis as suggested by longitudinal PET studies (Nandhagopal et al., 2011). Therefore, it is reasonable to expect such clinical correlations with the $SN_{VOL,QSM}$. The correlation was not significant between the global iron content and disease duration in the whole PD group but only significant in the subgroup during the first 5 years of disease duration. The increase in iron content is most likely due to the loss of at least the N1 sign and the increase in iron in that territory (Cheng et al., 2020).

However, no correlation was found between $SN_{VOL,MTC}$ and clinical scales even though it provided the highest AUC to differentiate early stage PD subjects from controls. The question of clinical correlation with imaging biomarkers is complicated since PD is a heterogeneous neurodegenerative condition with different genetics, pathology, clinical phenotypes and disease duration. In this work, only early stage PD subjects were recruited which means that a correlation with clinical data may not necessarily exist for these subjects. Ideally, we should be able to see correlations as subjects progress towards later stages of the disease. Furthermore, there is contradictory evidence in the literature regarding the correlation between NM measures and UPDRS-III scores. Some previous neuroimaging studies have shown significant correlations of NM volume with either UDPRS-III and/or disease duration (Isaias et al.,

2016; Matsuura et al., 2016; Schwarz et al., 2011; Schwarz et al., 2017; Wang et al., 2018a) while a few other papers were unable to find any clinical correlations with NM volume. (Castellanos et al., 2015; Hatano et al., 2017; Schwarz et al., 2017) Several pathological studies showed a loss of NM with the severity of the disease or disease duration in PD subjects. (Fearnley and Lees, 1991; Greffard et al., 2006; Kordower et al., 2013; Ma et al., 1997) These findings are consistent with a loss of NM as a representation of pathological changes in the SN of PD patients. On the other hand, while other studies have shown weak or moderate correlations between UPDRS-III scores and the NM signal area (Fabbri et al., 2017) or NM volume, (Kuya et al., 2018) another paper showed no association between the NM content and any of the above-mentioned clinical scores. (Pyatigorskaya et al., 2018) Therefore, given that we have a relatively small sample size of PD subjects going through their early stages and the fact that these clinical manifestations may vary across different populations, it is not surprising that we do not see such correlations. (see **Supplementary section S4**) We found no correlation of QSM values with UPDRS-III in this study, although such correlation has been seen before in the literature. (Du et al., 2018) However, in general, inconsistent results have been reported across studies with some papers reporting no correlation of QSM values with UPDRS-III. (Du et al., 2016; Langkammer et al., 2016) Since UPDRS-III measures motor performance at the time of the examination, (Harrison et al., 2009) this discrepancy of the correlation between QSM values and UPDRS-III scores among different studies can be partly caused by residual treatment effects at the time of motor examination.

The semi-automatic DP approach used in this study provides a means to obtain consistent final boundaries using different initial ROIs for the NM complex and SN. However, it should be noted that any automated or semi-automated method still has certain constraints associated with them that can potentially lead to changes in volumetric results. Specifically, one study by Ogisu et al. found that by using a region-growing semi-automated technique the NM volumes can substantially decrease as a function of increasing thresholds leading to poor separation between PD and HC at lower threshold values. (Ogisu et al., 2013) Given the CNR associated with the MTC and QSM images as well as the nature of the DP algorithm used here, this technique tends to produce boundaries and volumes close to those from the full width half maximum and, hence, will have an intermediate volume compared to methods using low or high thresholds. We also reviewed the DP boundaries to ensure that no artifacts or errors in the boundaries occurred. This was unlikely given that the initial boundaries were manually drawn. See the supplementary material (**Supplementary section S7** in particular) for a more in-depth discussion of volume measurements compared across different methods and different papers.

There are a few limitations in this work. First, the lack of definite diagnostic confirmation by neuropathologic assessment is a potential limitation. Nevertheless, all the PD subjects were followed up clinically for at least 12 months and the clinical diagnoses were confirmed. Second, the sample size was relatively small and for clinical adoption of this methodology; a much larger number of subjects will be required. Third, in order to accurately define the initial boundaries outside the final ROIs, the DP algorithm proposed in this study requires a priori knowledge of the anatomy of the structures in the midbrain. Fourth, one could use higher in-plane resolution to better define the boundaries of the ROIs, but it would come at the expense of increased scan time and less signal-to-noise as well as increased potential for patient motion. Fifth, this study only focused on differentiating early stage PD subjects from HCs but not differential diagnosis among parkinsonian disorders which is more challenging clinically. In the future, it will be interesting to investigate the differential diagnosis performance using this approach between PD and atypical parkinsonian syndromes.

In summary, we have introduced a rapid 3D imaging approach to depict NM degeneration and iron deposition simultaneously using a semi-automated boundary detection algorithm. Although the $SN_{VOL,MTC}$ had the highest AUC of the individual measures followed by the N1 sign with the second highest AUC, each measure plays a complementary role in evaluating PD with the $SN_{VOL,QSM}$ specifically correlating with UPDRS-III. This approach provides a practical MR imaging method to differentiate early stage subjects with PD from HCs with an AUC as high as .98. With minor changes in the sequence design, this multi-contrast GRE-based single MRI sequence has the potential to be implemented across all major manufacturers' equipment with a total acquisition time on the order of 5 minutes.

Credit authorship contribution statement

He, N.: Conceptualization; Writing – Original draft; Data curation; Investigation; Formal analysis; Funding acquisition. **Ghassaban, K.**: Writing – original draft; Data curation; Investigation; Formal analysis. **Pei, H.**: Writing – Review & Editing; Data curation; Investigation. **Jokar, M.**: Writing – original draft; Methodology; Formal analysis; Visualization. **Wang, Y.**: Writing – Review & Editing; Resources; Investigation. **Cheng, Z.**: Writing – Review & Editing; Resources; Investigation. **Jin, Z.**: Writing – Review & Editing; Resources; Investigation. **Li, Y.**: Writing – Review & Editing; Resources; Investigation. **Sethi, S.**: Writing – Review & Editing; Resources; Investigation. **He, Y.**: Writing – Review & Editing; Resources; Investigation. **Chen, Y.**: Writing – Review & Editing; Resources; Investigation. **Gharabaghi, S.**: Processing of acquired data and writing. **Chen, S.**: Conceptualization; Funding acquisition; Project administration; Investigation; Resources. **Yan, F.**: Conceptualization; Supervision; Funding acquisition; Resources; Writing – Review & Editing. **Haacke, E.M.**: Conceptualization; Writing – original draft; Supervision; Methodology.

Data and code availability statement

The source and means of obtaining the data used in this paper has been described in the Methods section of the paper. The codes used in this study are available upon a reasonable request from the corresponding author Yan, F. The data is available via a reasonable request with a formal data sharing agreement to the corresponding author Yan, F.

Acknowledgements

We thank Mr. Emil Pacurar for handling all the data issues and automatically processing STAGE data. We thank Dr. Jason Langley for his critical review. We thank Junchen Li for helping create the midbrain schematic. This work was supported, in part, by the National Natural Science Foundation of China (grant number: 81801652 for Naying He, M.D.; grant number: 81971576 for Fuhua Yan, M.D., Naying He, M.D., Zenghui Cheng, M.D.; grant numbers: 81430022, 91332107, and 81371407 for Shengdi Chen, M.D.; and grant number: 81801267 for Pei Huang, M.D.); a grant from the Science and Technology Commission of Shanghai Municipality (17411952700) for Fuhua Yan, M.D., Naying He, M.D., Zenghui Cheng, M.D., and Yan Li, M.S.; a grant from the Shanghai Sailing Program (18YF1414700) for Naying He, M.D. and Yan Li, M.S.; and the Innovative Research Team of High-level Local Universities in Shanghai.

Supplementary materials

Supplementary material associated with this article can be found, in the online version, at doi:10.1016/j.neuroimage.2021.117810.

References

Abdul-Rahman, H.S., Gdeisat, M.A., Burton, D.R., Lalor, M.J., Lilley, F., Moore, C.J., 2007. Fast and robust three-dimensional best path phase unwrapping algorithm. Appl Opt 46, 6623–6635.

Barrett, M.J., Wylie, S.A., Harrison, M.B., Wooten, G.F., 2011. Handedness and motor symptom asymmetry in Parkinson's disease. J. Neurol. Neurosurg. Psychiatry 82, 1122–1124.

Berg, D., Adler, C.H., Bloem, B.R., Chan, P., Gasser, T., Goetz, C.G., Halliday, G., Lang, A.E., Lewis, S., Li, Y., Liepelt-Scarfone, I., Litvan, I., Marek, K., Maetzler, C., Mi, T., Obeso, J., Oertel, W., Olanow, C.W., Poewe, W., Rios-Romenets, S., Schaffer, E., Seppi, K., Heim, B., Slow, E., Stern, M., Bledsoe, I.O., Deuschl, G., Postuma, R.B., 2018. Movement disorder society criteria for clinically established early Parkinson's disease. Mov. Disord. 33, 1643–1646.

Blazejewska, A.I., Schwarz, S.T., Pitiot, A., Stephenson, M.C., Lowe, J., Bajaj, N., Bowtell, R.W., Auer, D.P., Gowland, P.A., 2013. Visualization of nigrosome 1 and its loss in PD: pathoanatomical correlation and in vivo 7 T MRI. Neurology 81, 534–540.

Cassidy, C.M., Zucca, F.A., Girgis, R.R., Baker, S.C., Weinstein, J.J., Sharp, M.E., Bellei, C., Valmadre, A., Vanegas, N., Kegeles, L.S., Brucato, G., Jung Kang, U., Sulzer, D., Zecca, L., Abi-Dargham, A., Horga, G., 2019. Neuromelanin-sensitive MRI as a noninvasive proxy measure of dopamine function in the human brain. Proc Natl Acad Sci U S A 116, 5108–5117.

Castellanos, G., Fernandez-Seara, M.A., Lorenzo-Betancor, O., Ortega-Cubero, S., Puigvert, M., Uranga, J., Vidorreta, M., Irigoyen, J., Lorenzo, E., Munoz-Barrutia, A., Ortiz-de-Solorzano, C., Pastor, P., Pastor, M.A., 2015. Automated neuromelanin imaging as a diagnostic biomarker for Parkinson's disease. Mov. Disord. 30, 945–952.

Chen, Y., Liu, S., Wang, Y., Kang, Y., Haacke, E.M., 2018. STrategically Acquired Gradient Echo (STAGE) imaging, part I: creating enhanced T1 contrast and standardized susceptibility weighted imaging and quantitative susceptibility mapping. Magn. Reson. Imaging 46, 130–139.

Cheng, Z., He, N., Huang, P., Li, Y., Tang, R., Sethi, S.K., Ghassaban, K., Yerramsetty, K.K., Palutla, V.K., Chen, S., Yan, F., Haacke, E.M., 2020. Imaging the Nigrosome 1 in the substantia nigra using susceptibility weighted imaging and quantitative susceptibility mapping: an application to Parkinson's disease. Neuroimage Clin. 25, 102103.

Du, G., Lewis, M.M., Sica, C., He, L., Connor, J.R., Kong, L., Mailman, R.B., Huang, X., 2018. Distinct progression pattern of susceptibility MRI in the substantia nigra of Parkinson's patients. Mov. Disord. 33, 1423–1431.

Du, G., Liu, T., Lewis, M.M., Kong, L., Wang, Y., Connor, J., Mailman, R.B., Huang, X., 2016. Quantitative susceptibility mapping of the midbrain in Parkinson's disease. Mov. Disord. 31, 317–324.

Fabbri, M., Reimao, S., Carvalho, M., Nunes, R.G., Abreu, D., Guedes, L.C., Bouca, R., Lobo, P.P., Godinho, C., Coelho, M., Goncalves, N.C., Rosa, M.M., Antonini, A., Ferreira, J.J., 2017. Substantia nigra neuromelanin as an imaging biomarker of disease progression in Parkinson's disease. J. Parkinsons Dis. 7, 491–501.

Fearnley, J.M., Lees, A.J., 1991. Ageing and Parkinson's disease: substantia nigra regional selectivity. Brain 114 (Pt 5), 2283–2301.

Ghassaban, K., Liu, S., Jiang, C., Haacke, E.M., 2019. Quantifying iron content in magnetic resonance imaging. Neuroimage 187, 77–92.

Goetz, C.G., Tilley, B.C., Shaftman, S.R., Stebbins, G.T., Fahn, S., Martinez-Martin, P., Poewe, W., Sampaio, C., Stern, M.B., Dodel, R., Dubois, B., Holloway, R., Jankovic, J., Kulisevsky, J., Lang, A.E., Lees, A., Leurgans, S., LeWitt, P.A., Nyenhuis, D., Olanow, C.W., Rascol, O., Schrag, A., Teresi, J.A., van Hilten, J.J., LaPelle, N.Movement Disorder Society, U.R.T.F., 2008. Movement disorder society-sponsored revision of the unified Parkinson's disease rating scale (MDS-UPDRS): scale presentation and clinimetric testing results. Mov Disord 23, 2129–2170.

Greffard, S., Verny, M., Bonnet, A.M., Beinis, J.Y., Gallinari, C., Meaume, S., Piette, F., Hauw, J.J., Duyckaerts, C., 2006. Motor score of the unified Parkinson disease rating scale as a good predictor of Lewy body-associated neuronal loss in the substantia nigra. Arch Neurol 63, 584–588.

Haacke, E.M., Chen, Y., Utriainen, D., Wu, B., Wang, Y., Xia, S., He, N., Zhang, C., Wang, X., Lagana, M.M., Luo, Y., Fatemi, A., Liu, S., Gharabaghi, S., Wu, D., Sethi, S.K., Huang, F., Sun, T., Qu, F., Yadav, B.K., Ma, X., Bai, Y., Wang, M., Cheng, J., Yan, F., 2020. Strategically acquired gradient echo (STAGE) imaging, part III: Technical advances and clinical applications of a rapid multi-contrast multi-parametric brain imaging method. Magn. Reson. Imaging 65, 15–26.

Haacke, E.M., Tang, J., Neelavalli, J., Cheng, Y.C., 2010. Susceptibility mapping as a means to visualize veins and quantify oxygen saturation. J. Magn. Reson. Imaging 32, 663–676.

Harrison, M.B., Wylie, S.A., Frysinger, R.C., Patrie, J.T., Huss, D.S., Currie, L.J., Wooten, G.F., 2009. UPDRS activity of daily living score as a marker of Parkinson's disease progression. Mov. Disord. 24, 224–230.

Hatano, T., Okuzumi, A., Kamagata, K., Daida, K., Taniguchi, D., Hori, M., Yoshino, H., Aoki, S., Hattori, N., 2017. Neuromelanin MRI is useful for monitoring motor complications in Parkinson's and PARK2 disease. J. Neural. Transm. (Vienna) 124, 407–415.

He, N., Langley, J., Huddleston, D.E., Chen, S., Huang, P., Ling, H., Yan, F., Hu, X., 2020. Increased iron-deposition in lateral-ventral substantia nigra pars compacta: a promising neuroimaging marker for Parkinson's disease. Neuroimage Clin. 28, 102391.

Huddleston, D.E., Langley, J., Sedlacik, J., Boelmans, K., Factor, S.A., Hu, X.P., 2017. In vivo detection of lateral-ventral tier nigral degeneration in Parkinson's disease. Hum. Brain Mapp. 38, 2627–2634.

Isaias, I.U., Trujillo, P., Summers, P., Marotta, G., Mainardi, L., Pezzoli, G., Zecca, L., Costa, A., 2016. Neuromelanin imaging and dopaminergic loss in parkinson's disease. Front. Aging Neurosci. 8, 196.

Jiang, J., Haacke, E.M., Dong, M., 2007. Dependence of vessel area accuracy and precision as a function of MR imaging parameters and boundary detection algorithm. J. Magn. Reson Imaging 25, 1226–1234.

Keren, N.I., Taheri, S., Vazey, E.M., Morgan, P.S., Granholm, A.C., Aston-Jones, G.S., Eckert, M.A., 2015. Histologic validation of locus coeruleus MRI contrast in post-mortem tissue. Neuroimage 113, 235–245.

Kordower, J.H., Olanow, C.W., Dodiya, H.B., Chu, Y., Beach, T.G., Adler, C.H., Halliday, G.M., Bartus, R.T., 2013. Disease duration and the integrity of the nigrostriatal system in Parkinson's disease. Brain 136, 2419–2431.

Kuya, K., Ogawa, T., Shinohara, Y., Ishibashi, M., Fujii, S., Mukuda, N., Tanabe, Y., 2018. Evaluation of Parkinson's disease by neuromelanin-sensitive magnetic resonance imaging and (123)I-FP-CIT SPECT. Acta. Radiol. 59, 593–598.

Langkammer, C., Pirpamer, L., Seiler, S., Deistung, A., Schweser, F., Franthal, S., Homayoon, N., Katschnig-Winter, P., Koegl-Wallner, M., Pendl, T., Stoegerer, E.M., Wenzel, K., Fazekas, F., Ropele, S., Reichenbach, J.R., Schmidt, R., Schwingenschuh, P., 2016. Quantitative susceptibility mapping in Parkinson's disease. PLoS One 11, e0162460.

Langley, J., Huddleston, D.E., Chen, X., Sedlacik, J., Zachariah, N., Hu, X., 2015. A multicontrast approach for comprehensive imaging of substantia nigra. Neuroimage 112, 7–13.

Langley, J., Huddleston, D.E., Sedlacik, J., Boelmans, K., Hu, X.P., 2017. Parkinson's disease-related increase of T2*-weighted hypointensity in substantia nigra pars compacta. Mov. Disord. 32, 441–449.

Lee, H., Baek, S.Y., Chun, S.Y., Lee, J.H., Cho, H., 2018. Specific visualization of neuromelanin-iron complex and ferric iron in the human post-mortem substantia nigra using MR relaxometry at 7T. Neuroimage 172, 874–885.

Lehericy, S., Bardinet, E., Poupon, C., Vidailhet, M., Francois, C., 2014. 7 Tesla magnetic resonance imaging: a closer look at substantia nigra anatomy in Parkinson's disease. Mov. Disord. 29, 1574–1581.

Liu, M., Liu, S., Ghassaban, K., Zheng, W., Dicicco, D., Miao, Y., Habib, C., Jazmati, T., Haacke, E.M., 2016. Assessing global and regional iron content in deep gray matter as a function of age using susceptibility mapping. J. Magn. Reson. Imaging 44, 59–71.

Liu, S., Mok, K., Neelavalli, J., Cheng, Y.C., Tang, J., Ye, Y., Haacke, E.M., 2014. Improved MR venography using quantitative susceptibility-weighted imaging. J. Magn. Reson Imaging 40, 698–708.

Liu, Y., Li, J., He, N., Chen, Y., Jin, Z., Yan, F., Haacke, E.M., 2020. Optimizing neuromelanin contrast in the substantia nigra and locus coeruleus using a magnetization transfer contrast prepared 3D gradient recalled echo sequence. Neuroimage 218, 116935.

Ma, S.Y., Roytta, M., Rinne, J.O., Collan, Y., Rinne, U.K., 1997. Correlation between neuromorphometry in the substantia nigra and clinical features in Parkinson's disease using disector counts. J. Neurol. Sci. 151, 83–87.

Mahlknecht, P., Krismer, F., Poewe, W., Seppi, K., 2017. Meta-analysis of dorsolateral nigral hyperintensity on magnetic resonance imaging as a marker for Parkinson's disease. Mov. Disord. 32, 619–623.

Matsuura, K., Maeda, M., Tabei, K.I., Umino, M., Kajikawa, H., Satoh, M., Kida, H., Tomimoto, H., 2016. A longitudinal study of neuromelanin-sensitive magnetic resonance imaging in Parkinson's disease. Neurosci. Lett. 633, 112–117.

Nam, Y., Gho, S.M., Kim, D.H., Kim, E.Y., Lee, J., 2017. Imaging of nigrosome 1 in substantia nigra at 3T using multiecho susceptibility map-weighted imaging (SMWI). J. Magn. Reson. Imaging 46, 528–536.

Nandhagopal, R., Kuramoto, L., Schulzer, M., Mak, E., Cragg, J., McKenzie, J., McCormick, S., Ruth, T.J., Sossi, V., de la Fuente-Fernandez, R., Stoessl, A.J., 2011. Longitudinal evolution of compensatory changes in striatal dopamine processing in Parkinson's disease. Brain 134, 3290–3298.

Ogisu, K., Kudo, K., Sasaki, M., Sakushima, K., Yabe, I., Sasaki, H., Terae, S., Nakanishi, M., Shirato, H., 2013. 3D neuromelanin-sensitive magnetic resonance imaging with semi-automated volume measurement of the substantia nigra pars compacta for diagnosis of Parkinson's disease. Neuroradiology 55, 719–724.

Pavese, N., Tai, Y.F., 2018. Nigrosome imaging and neuromelanin sensitive MRI in diagnostic evaluation of parkinsonism. Mov Disord Clin Pract 5, 131–140.

Peran, P., Cherubini, A., Assogna, F., Piras, F., Quattrocchi, C., Peppe, A., Celsis, P., Rascol, O., Demonet, J.F., Stefani, A., Pierantozzi, M., Pontieri, F.E., Caltagirone, C., Spalletta, G., Sabatini, U., 2010. Magnetic resonance imaging markers of Parkinson's disease nigrostriatal signature. Brain 133, 3423–3433.

Prasad, S., Stezin, A., Lenka, A., George, L., Saini, J., Yadav, R., Pal, P.K., 2018. Three--dimensional neuromelanin-sensitive magnetic resonance imaging of the substantia nigra in Parkinson's disease. Eur. J. Neurol. 25, 680–686.

Pyatigorskaya, N., Magnin, B., Mongin, M., Yahia-Cherif, L., Valabregue, R., Arnaldi, D., Ewenczyk, C., Poupon, C., Vidailhet, M., Lehericy, S., 2018. Comparative study of MRI biomarkers in the substantia nigra to discriminate idiopathic Parkinson disease. AJNR Am. J. Neuroradiol. 39, 1460–1467.

Reimao, S., Ferreira, S., Nunes, R.G., Pita Lobo, P., Neutel, D., Abreu, D., Goncalves, N., Campos, J., Ferreira, J.J., 2016. Magnetic resonance correlation of iron content with neuromelanin in the substantia nigra of early-stage Parkinson's disease. Eur J Neurol 23, 368–374.

Reimao, S., Pita Lobo, P., Neutel, D., Correia Guedes, L., Coelho, M., Rosa, M.M., Ferreira, J., Abreu, D., Goncalves, N., Morgado, C., Nunes, R.G., Campos, J., Ferreira, J.J., 2015a. Substantia nigra neuromelanin magnetic resonance imaging in de novo Parkinson's disease patients. Eur. J. Neurol. 22, 540–546.

Reimao, S., Pita Lobo, P., Neutel, D., Guedes, L.C., Coelho, M., Rosa, M.M., Ferreira, J., Abreu, D., Goncalves, N., Morgado, C., Nunes, R.G., Campos, J., Ferreira, J.J., 2015b. Quantitative analysis versus visual assessment of neuromelanin mr imaging for the diagnosis of Parkinson's disease. J. Parkinsons Dis. 5, 561–567.

Schwarz, S.T., Rittman, T., Gontu, V., Morgan, P.S., Bajaj, N., Auer, D.P., 2011. T1-weighted MRI shows stage-dependent substantia nigra signal loss in Parkinson's disease. Mov Disord. 26, 1633–1638.

Schwarz, S.T., Xing, Y., Tomar, P., Bajaj, N., Auer, D.P., 2017. In vivo assessment of brainstem depigmentation in parkinson disease: potential as a severity marker for multicenter studies. Radiology 283, 789–798.

Schweser, F., Deistung, A., Lehr, B.W., Reichenbach, J.R., 2011. Quantitative imaging of intrinsic magnetic tissue properties using MRI signal phase: an approach to in vivo brain iron metabolism? Neuroimage 54, 2789–2807.

Sethi, S.K., Kisch, S.J., Ghassaban, K., Rajput, A., Rajput, A., Babyn, P.S., Liu, S., Szkup, P., Mark Haacke, E., 2019. Iron quantification in Parkinson's disease using an age-based

threshold on susceptibility maps: the advantage of local versus entire structure iron content measurements. Magn. Reson Imaging 55, 145–152.
Shinde, S., Prasad, S., Saboo, Y., Kaushick, R., Saini, J., Pal, P.K., Ingalhalikar, M., 2019. Predictive markers for Parkinson's disease using deep neural nets on neuromelanin sensitive MRI. Neuroimage Clin. 22, 101748.
Smith, S.M., 2002. Fast robust automated brain extraction. Hum Brain Mapp. 17, 143–155.
Stoeck, C.T., Hu, P., Peters, D.C., Kissinger, K.V., Goddu, B., Goepfert, L., Ngo, L., Manning, W.J., Kozerke, S., Nezafat, R., 2010. Optimization of on-resonant magnetization transfer contrast in coronary vein MRI. Magn. Reson Med. 64, 1849–1854.
Sulzer, D., Cassidy, C., Horga, G., Kang, U.J., Fahn, S., Casella, L., Pezzoli, G., Langley, J., Hu, X.P., Zucca, F.A., Isaias, I.U., Zecca, L., 2018. Neuromelanin detection by magnetic resonance imaging (MRI) and its promise as a biomarker for Parkinson's disease. NPJ Parkinsons Dis. 4, 11.
Takahashi, H., Watanabe, Y., Tanaka, H., Mihara, M., Mochizuki, H., Liu, T., Wang, Y., Tomiyama, N., 2018a. Quantifying changes in nigrosomes using quantitative susceptibility mapping and neuromelanin imaging for the diagnosis of early-stage Parkinson's disease. Br. J. Radiol. 91, 20180037.
Takahashi, H., Watanabe, Y., Tanaka, H., Mihara, M., Mochizuki, H., Takahashi, K., Yamamoto, K., Liu, T., Wang, Y., Tomiyama, N., 2018b. Comprehensive MRI quantification of the substantia nigra pars compacta in Parkinson's disease. Eur. J. Radiol. 109, 48–56.
Tang, J., Liu, S., Neelavalli, J., Cheng, Y.C., Buch, S., Haacke, E.M., 2013. Improving susceptibility mapping using a threshold-based K-space/image domain iterative reconstruction approach. Magn. Reson. Med. 69, 1396–1407.
Taniguchi, D., Hatano, T., Kamagata, K., Okuzumi, A., Oji, Y., Mori, A., Hori, M., Aoki, S., Hattori, N., 2018. Neuromelanin imaging and midbrain volumetry in progressive supranuclear palsy and Parkinson's disease. Mov. Disord. 33, 1488–1492.
Trutti, A.C., Mulder, M.J., Hommel, B., Forstmann, B.U., 2019. Functional neuroanatomical review of the ventral tegmental area. Neuroimage 191, 258–268.
Wang, J., Li, Y., Huang, Z., Wan, W., Zhang, Y., Wang, C., Cheng, X., Ye, F., Liu, K., Fei, G., Zeng, M., Jin, L., 2018a. Neuromelanin-sensitive magnetic resonance imaging features of the substantia nigra and locus coeruleus in de novo Parkinson's disease and its phenotypes. Eur. J. Neurol. 25, 949–e973.
Wang, X., Zhang, Y., Zhu, C., Li, G., Kang, J., Chen, F., Yang, L., 2019. The diagnostic value of SNpc using NM-MRI in Parkinson's disease: meta-analysis. Neurol. Sci..
Wang, Y., Chen, Y., Wu, D., Wang, Y., Sethi, S.K., Yang, G., Xie, H., Xia, S., Haacke, E.M., 2018b. Strategically acquired gradient echo (STAGE) imaging, part II: correcting for RF inhomogeneities in estimating T1 and proton density. Magn. Reson. Imaging 46, 140–150.
Yetnikoff, L., Lavezzi, H.N., Reichard, R.A., Zahm, D.S., 2014. An update on the connections of the ventral mesencephalic dopaminergic complex. Neuroscience 282, 23–48.